Eur Biophys J (2009) 38:1035–1047
DOI 10.1007/s00249-009-0506-1

ORIGINAL PAPER

Critical stresses for cancer cell detachment in microchannels

Cécile Couzon · Alain Duperray · Claude Verdier

Received: 16 March 2009 / Revised: 5 June 2009 / Accepted: 8 June 2009 / Published online: 5 July 2009

Abstract We present experiments involving cancer cells adhering to microchannels, subjected to increasing shear stresses (0.1–30 Pa). Morphological studies were carried out at different shear stresses. Cells exhibit spreading patterns similar to those observed under static conditions, as long as the shear stress is not too high. At critical wall shear stresses (around 2−5 Pa), cell-substrate contact area decreases until detachment at the larger stresses. Critical shear stresses are found to be lower for higher confinements (i.e. smaller cell height to channel height ratio). Fluorescent techniques were used to locate focal adhesions (typically 1 μm^2 in size) under various shearing conditions, showing that cells increase the number of focal contacts in the region facing the flow. To analyze such data, we propose a model to determine the critical stress, resulting from the competition between hydrodynamic forces and the adhesive cell resistance. With this model, typical adhesive stresses exerted at each focal contact can be determined and are in agreement with previous works.

Keywords Microfluidics · Cancer cells · Critical stress · Focal adhesions

C. Couzon · C. Verdier (✉)
Laboratoire de Spectrométrie Physique (UMR 5588),
CNRS, Université Grenoble I, 140 avenue de la physique,
BP 87, 38402 Saint-Martin d'Hères cedex, France
e-mail: verdier@ujf-grenoble.fr

A. Duperray
INSERM U823, Rond-point de la Chantourne,
38706 La Tronche cedex, France

A. Duperray
Faculté de Médecine, Institut d'oncologie/développement
Albert Bonniot et Institut Français du Sang (UMR S823),
Université Joseph Fourier-Grenoble I, Grenoble, France

Introduction

The response of cells to mechanical stresses is a key factor in many biological processes, for example cell division, embryogenesis, cell migration, diapedesis, etc. Typical examples concern the reaction to shear stresses exerted as cells travel through the blood, or when they adhere to the vascular wall, but also within tissues, because cells are submitted to various forces due to the environment. To a first approximation, cells exert a different response as a function of substrate stiffness (Discher et al. 2005) and develop stronger forces when the substrate is more rigid (Lo et al. 2000). They also develop larger forces as they spread (De et al. 2007; Reinhart-King et al. 2005) or as the ligand concentration increases. Cells might also change their orientation as a function of environmental anisotropy, leading to cell polarization as shown in recent experiments on specific micropatterned surfaces (Théry et al. 2006). But their orientation might also depend on the type of forces to which they are subjected, like static, quasistatic, or periodic stresses (De et al. 2007). Reaction to mechanical stresses involves mechanotransduction, or how forces are converted into biochemical and functional responses. This transduction of external forces into an adapted cell behavior requires first sensing of external forces, then transmission of forces from outside the cell through cell–matrix and cell–cell contacts, leading to the initiation of intracellular signaling cascades that alter cellular behaviors. Although some aspects of this machinery remain unclear, it is known that dynamic feedback takes place implying external mechanical force, signaling, and internal force, which lead to the reorganization of the cytoskeleton, and the formation or disruption of focal adhesions (Chen 2008; Ingber 2003; Orr et al. 2006). For example focal contacts can act as mechanosensors and enable growth of

further adhesion sites (Riveline et al. 2001) in the case of adhering fibroblasts. An additional effect is the actin reorganization of a cell under flow, as shown for example with *Dyctiostelium discoideum* (Dalous et al. 2008). Flow reversal leads to a change in cell polarity, corresponding to relocalization of an actin-rich region opposite to the flow. In other words, cells are able to modify their local rheological properties (Verdier 2003) in order to achieve a particular response.

Many experiments have been conducted in the past to study cell behavior under flow, a specific way of applying mechanical stresses to adhering cells. This aspect is particularly important when trying to model leukocyte–cancer cell interactions with the endothelium (Jin et al. 2007; Verdier et al. 2009). First, interaction with the endothelium is followed by cell activation and formation of weak bonds leading to cell rolling (Lawrence and Springer 1991) followed by mechanotransduction and the formation of stronger bonds, allowing cells to adhere, spread, and, eventually, transmigrate across the endothelial monolayer. During this process, it is important to determine which forces are necessary to detach such bonds (i.e. when tumor cells adhere to the endothelium), and to determine the force and/or the number of bonds needed for the cell to resist the flow (Chotard-Ghodsnia et al. 2007). Another important application is the transport of cells in microchannels which is now becoming very promising, especially with recent advances of microfluidics which could allow the sorting of normal cells from cancer cells. Experiments on the influence of a controlled flow rate (or shear stress) on adhering cells have been performed in parallel plate flow chambers (Pierres et al. 1995; Cao et al. 1998; Chotard-Ghodsnia et al. 2002; Das et al. 2008) or radial flow experiments (Decave et al. 2002), or with micropipettes (Moazzam et al. 1997; Coughlin and Schmid-Schönbein 2004; Bohnet et al. 2006). Such devices enable control of the applied shear stresses, usually chosen in the range (0.1–2 Pa) as in physiological conditions. Particular attention has been given to endothelial cells under flow conditions. Thoumine et al. (1995) showed that endothelial cells become elongated in the flow direction in an almost regular manner, and that the underlying actin cytoskeleton also aligns in the same direction. Chachisvilis et al. (2006) finally demonstrated the role of G-protein-coupled receptors, which act as mechanosensors, as was shown before for other proteins such as integrins and cadherins (Schwartz and DeSimone 2008).

To further investigate the response of a cell exposed to a flow field, it is necessary to find out theoretically which forces and torques are applied to the adhering cell, depending on flow geometry. Pozrikidis (1997) determined numerically forces and torques exerted by a 3D shear flow on an adhering cell, assuming the cell to be a spherical cap or an ellipsoid, but the study was limited to an infinite flow domain. Gaver and Kute (1988) studied analytically and numerically the effect of flow on a 2D adherent cell in a microchannel and generalized this idea to the 3D case, coming up with simple formulas depending on confinement. The confinement R/h, i.e. the ratio between cell height (R) and channel height (h), determines how the cell obstructs the microchannel, $R/h \to 1$ meaning that the cell blocks the channel whereas $R/h \to 0$ means a high channel or a small cell. Once the flow field is known, models of adhesion and detachment can then enable determination of dissociation rate constants (Hammer and Lauffenburger 1987), because cell detachment is controlled by the ability of cells to form bonds between their receptors and the corresponding ligands on the surface. The precise mechanisms by which cells spread and adhere under flow are not yet known.

Therefore the purpose of this study is to focus on experimental results where cells adhering to the walls of a microchannel are subjected to an increasing shear flow until detachment. This implies modifications of the morphology of the cells, in relation to their adhesion properties and the flow characteristics. This is not only relevant for microfluidics, but is also a true situation encountered in post capillary venules (5−200 μm in size) where circulating cells interact with the vessel walls and adhere. Recent developments have enabled the study of cell migration (Saadi et al. 2006; Chaw et al. 2007; Irima et al. 2007) and adhesion strength (Lu et al. 2004; Wankhede et al. 2006; Gutierrez and Groisman 2007; Kwon et al. 2007) in confined geometries. Most of these studies consist in end-point assays, i.e. measurement of the total distance the cells migrate or counting the fraction of remaining adherent cells at the end of the experiment. The motivation here is to analyze cell behavior carefully, in particular the exact stresses or forces necessary to achieve cell detachment, and how this can be related to cell adhesion. We will focus on a particular type of cancer cells (T24, an epithelial bladder type) and investigate the action of a flow field while comparing it with the adhesion sites formed below the cell. This study can serve as an interesting tool for estimating the typical force per adhesion site by which this type of cell adheres to a given substrate. This can be obtained by fluorescence microscopic observation of focal adhesions, enabling counting of such adhesion sites and their size.

The paper is organized as follows. In the first part, we describe "Materials and methods", in particular cells, microchannels build-up, fluorescence microscopy, and the working equations governing flow. Then results are collected to describe cell spreading and detachment, in order to propose a new method for determining the critical stress

for cell retraction. In the final part, the effect of confinement on the critical shear stress is discussed; we then use a model based on previous work (Gaver and Kute 1988) to interpret our data and come up with the missing values in the adhesion model. This enables us to determine typical forces involved at each focal adhesion site. Such results obtained for this type of cell are then compared with those from previous studies.

Materials and methods

Cell culture

T24 is a human epithelial bladder cancer cell line (ATCC No HBT-4). In our experiments, T24 cells were cultured in 25 cm^2 tissue-culture flasks (T25) at 37°C, in a humidified atmosphere with 5% CO_2. The cells were incubated in RPMI supplemented with 100 U/mL penicillin, 100 μg/mL streptomycin, and 10% fetal calf serum. Cells were grown to near confluence in the culture flasks and then suspended with 0.05% trypsin–EDTA solution. The concentration of suspended cells was determined using a Neubauer cell, before being introduced into the microchannels.

Long term experiments under static conditions

T24 cells in culture medium were placed on a glass slide covered with a thin layer of PDMS (<0.5 mm). Culture medium height was roughly 1.5 mm. Cells were left to sediment and spread under static conditions. Phase-contrast images were taken every 5 min. The substrate and the coating were the same as those used in microchannels, consequently these experiments under static conditions can be used as a control for the experiments under flow conditions.

Design of microfluidic devices

The microfluidic devices were made using the PDMS rapid photolithographic technique, in accordance with previous work (Duffy et al. 1988). The photolithography masks bearing the channel design were printed on high-resolution films. The negative masters were then created from a photo-patternable epoxy (SU-8, Gersteltec) spin-coated on to silicon wafers, and exposed to UV light through the film negative of the desired channel size. The silicon was then etched with inverse structures of the microfluidic channels: typically 1 mm wide (w) and 50–300 μm high (h, measured by scanning electron microscopy, SEM, afterwards). The PDMS elastomer devices were molded from the masters using two-part Sylgard silicon elastomer (a mixture of 1:10 silicon elastomer and curing agent degassed and poured against the silicon master). Once cured, each PDMS device was punched with inlet/outlet holes, treated with air plasma (2×10^{-4} bar at 6.8 W coil power for 40 s), bonded to the glass slide by putting both treated surfaces in contact to each other immediately after, and connected to tubes which were sealed with glue (Araldite). In order to prevent bubbles from entering the channel, a bubble trap was also included in the microfluidic device, as shown in Fig. 1.

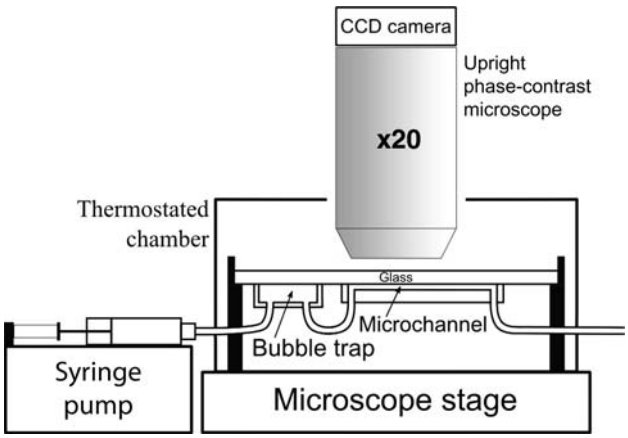

Fig. 1 Full view of the experimental set-up. The microfluidic device is placed in a thermostated chamber at 37°C under the ×20 objective of an upright phase-contrast microscope. Fluid flow is controlled by a syringe-pump. Before reaching the microchannel, the fluid first passes through the bubble trap (completely filled with medium before the experiment), where bubbles remain trapped

Channel coating and cell loading for shearing experiments

Prior to each experiment, the microchannel walls were functionalized with a fibronectin solution (20 μg/mL) for 1 h at a typical flow rate of 0.8 mL/h in order to allow fibronectin adsorption on to the treated PDMS surfaces. The bubble trap was then filled with culture medium. Finally the channel was rinsed for 15 min with culture medium.

Cells (diameter ~15 μm) in suspension at a concentration adapted to the channel size (in the range $1-5.0 \times 10^6$ cells/mL, or an equivalent volume concentration of 0.05−0.28%) were pumped into a microfluidic device at a low flow rate Q corresponding to a small wall shear stress (WSS) (in the connection tube) less than 0.1 Pa. Typically $Q = 10$ mL/h in a cylinder of radius $r = 0.4$ mm, $\eta \sim 10^{-3}$ Pa s at 37°C, which leads to a WSS in the connection tube $\sigma = 4\eta Q/\pi\ r^3 = 0.055$ Pa. Once located in the channel, cells were left at rest for 15 min to allow attachment to the channel wall.

Experiments under controlled flow conditions

Shearing experiments were performed to investigate the responses of cells and their ability to resist the flow. In particular, measurement of the cell area over a range of shear stresses is important to determining the effect of flow on adherent cells. During measurements, a continuous flow was applied and a region of interest (ROI) in the center of the channel was investigated at fixed time intervals (15 s). The flow rate was changed regularly every 5 min, starting at low flow rates and then increasing, inducing higher shear stresses progressively. In all cases, the Reynolds number given by $Re = \rho V D_h/\eta$ was less than 130 (where $D_h = wh/2(w+h)$ is the hydraulic diameter and V the mean fluid velocity), indicating that the flow was laminar. Images were taken at the center of the channel, away from the side walls, to ensure the full development of the velocity profile. Individual cell morphologies (area, angle, aspect ratio, etc.) were recorded in real time using phase contrast microscopy. A global view of the experimental set-up can be seen in Fig. 1.

Determination of the wall shear stress (no cell)

To determine the WSS with no cell in the channel, the stress vector on an oriented facet (normal unit vector $\vec{n}$) is introduced: $\vec{t}(\vec{n}) = \Sigma.\vec{n}$. Σ is the shear stress tensor, given by $\Sigma = -p\mathbf{I} + 2\eta\mathbf{D}$ for a Newtonian incompressible fluid, η the fluid viscosity, $\mathbf{D}$ the symmetrical part of the fluid velocity gradient tensor and p the pressure. $\vec{v}$ is the fluid velocity and only has a z-component depending on x and y, in the coordinate system shown in Fig. 2 because of the translational invariance. Note that the cell is shown in order for this figure to be used later on, although the channel is now empty.

Consequently the shear stress depends on the velocity field $\vec{v}$ which is described by the steady Navier–Stokes equations. In the case of an incompressible Newtonian fluid, the fluid velocity $\vec{v}$ and the pressure p are solutions of the system:

$$\begin{cases} \operatorname{div}\vec{v} = 0 \\ \rho\,(\operatorname{grad}\vec{v})\,\vec{v} = -\overrightarrow{\operatorname{grad}p} + \eta\Delta\vec{v} \end{cases} \quad (1)$$

together with boundary conditions $\vec{v}(-\frac{w}{2}, y, z) = \vec{v}(\frac{w}{2}, y, z) = \vec{v}(x, 0, z) = \vec{v}(x, h, z) = \vec{0}$, where ρ is the fluid density.

The previous system (Eq. 1) can be solved for the only component $v_z(x, y)$ by using Fourier series decomposition (White 2003). Assuming a constant pressure gradient $\Delta p/L$ (where Δp is the pressure drop over the length of the channel L) corresponding to the channel sketched in Fig. 2, the solution reads:

$$v_z(x,y) = \frac{\Delta p}{\eta L}\frac{4h^2}{\pi^3}\sum_{n=1,3,\ldots,}^{\infty}\frac{1}{n^3}\left(1 - \frac{\cosh\left(\frac{n\pi x}{h}\right)}{\cosh\left(\frac{n\pi w}{2h}\right)}\right)\sin\left(\frac{n\pi y}{h}\right) \quad (2)$$

with $-w/2 < x < w/2$ and $0 < y < h$.

This enables determination of the component of the stress tensor Σ of interest, i.e. $\sigma_{zy} = \eta\frac{\partial v_z}{\partial y}$, related to the WSS at $y = 0$ in the absence of cells:

$$\sigma_{zy} = \frac{\eta Q\pi^2}{2h^2}\frac{\sum_{n=1,3,\ldots,}^{\infty}\left[\frac{1}{n^2}\left(1 - \frac{\cosh\left(\frac{n\pi x}{h}\right)}{\cosh\left(\frac{n\pi w}{2h}\right)}\right)\cos\left(\frac{n\pi y}{h}\right)\right]}{\sum_{n=1,3,5,\ldots,}^{\infty}\frac{1}{n^4}\left[w - \frac{2h}{n\pi}\tanh\left(\frac{wn\pi}{2h}\right)\right]} \quad (3)$$

where Q is flow rate, and w and h are, respectively, the channel width and height. σ_{zy} is the stress felt by the cell if it were flat, because it corresponds to the main shear forces exerted by the fluid. We will see in the final section that this value can be affected by the presence of a cell. To determine the evolution of the WSS in the microchannel, calculations were performed with Scilab software.

For a thin channel ($w \gg h$), Eq. 3 can be simplified and the WSS has an almost constant value across the channel x-axis (except in a narrow region close to the vertical edges) given by Eq. 4 and also shown in Fig. 3.

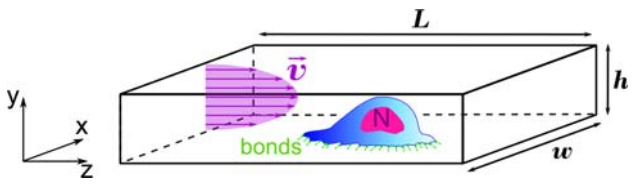

Fig. 2 Schematic view of the microchannel (height h, width w and length L) used in the experiments, with a cell (nucleus N) adhering to the bottom wall. The system of coordinates chosen to describe the flow field ($-w/2 < x < w/2$, $0 < y < h$ and $0 < z < L$) and the velocity profile in a cell-free channel are represented on the left

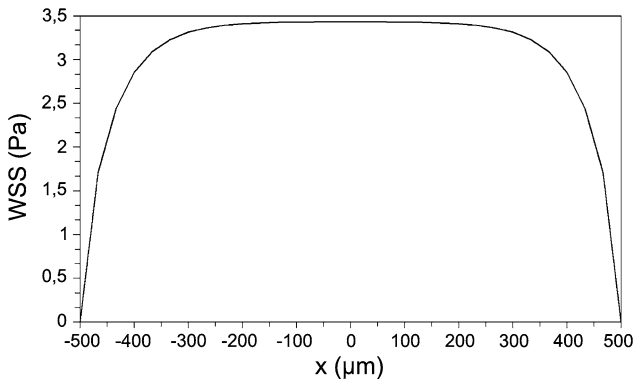

Fig. 3 $\sigma_{zy}(x, 0, z)$ WSS at the bottom of a parallelepipedic channel ($w = 1$ mm, $h = 200$ µm, $Q = 2 \times 10^{-8}$ m^3 s^{-1}). The WSS is almost constant across the x axis, except in the regions close to the vertical walls

$$\sigma_{zy} = \frac{6\eta Q}{wh^2} \quad (4)$$

This is usually a good assumption in our experiments, with w of the order of 1 mm and h ranging between 50 and 250 μm.

Data analysis

Measurements were done on time-lapse images of the cells by drawing contours using a graphical pad (Fig. 4). The plane of focus was chosen to be the plane of location of the cell–substrate contact area. The resolution of the images using a ×20 microscope objective for such phase contrast images was 3.1 pixels/μm and a depth of field around 3 μm. Area (i.e. cell–substrate contact area), perimeter, circularity, and ellipse properties (axes, angle) were obtained by use of ImageJ software (NIH Image, Bethesda, USA). Measurements were repeated several times and led to an uncertainty of 5% maximum for the contact area. The cell area $A(t)$ was plotted versus time as shown, for instance, in Fig. 5 (flow rate increased every 5 min). $A(t)$ was fitted by a polynomial and the mean slope was calculated from this polynomial fit for each flow rate corresponding to a determined WSS. Thus the slope $\frac{dA}{dt}$ (corresponding to the area change) was plotted versus the WSS for each value of the applied flow rate or WSS giving rise to discrete data. Because the applied duration of each flow rate was short, sufficient data could be obtained for determination of the critical value of the WSS (i.e. WSS_c), this value being the WSS that gives a zero-slope, and therefore maximum in cell area.

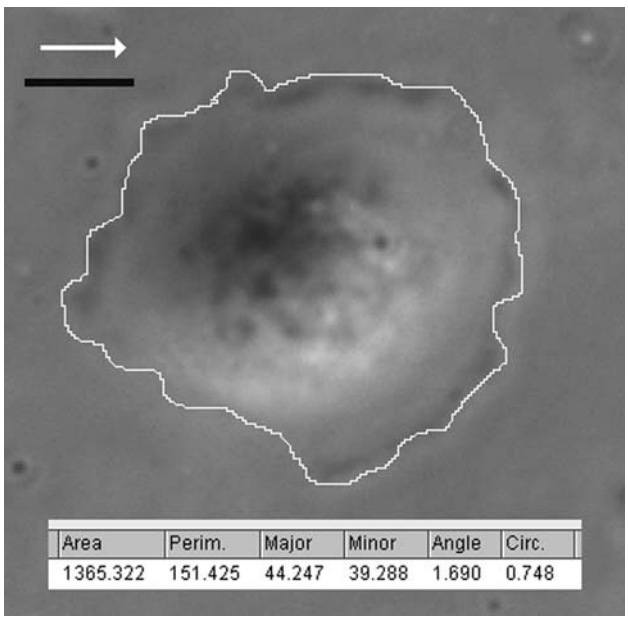

Fig. 4 Contour of T24 cell drawn with a graphic pad and measurement of cell properties (area, perimeter, ellipse axes and orientation angle, circularity index defined as $\frac{4\pi \text{ area}}{\text{perimeter}^2}$). The nucleus of the cell is surrounded by the lamellipodium. *White arrow* shows the flow direction. The *black scale* represents 10 μm. Channel dimensions: $h = 82$ μm, $w = 1$ mm, WSS = 0.26 Pa

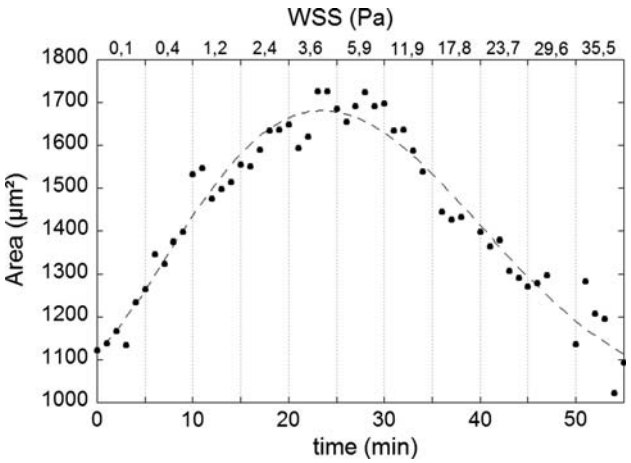

Fig. 5 Area versus time $A(t)$ for a T24 cell adhering to the bottom wall of a microchannel ($w = 1$ mm, $h = 61$ μm) and submitted to a flow increasing every 5 min. The *black dots* represent measurements obtained by use of ImageJ software and the thin *dashed line* is a polynomial fit. Wall shear stress values are given on the top axis

Immunofluorescence

Fluorescence experiments, based on immunofluorescence recognition of the paxillin molecule involved in the focal adhesion complexes, have been used to locate focal adhesions on the adherent cells submitted to flow in the microchannel. Fluorescence images were obtained with a ×40 microscope objective at 6 pixels/μm resolution and a depth of field of roughly 2 μm. Cells have been fixed at different steps during the shear stress increase consisting of four plateaux, corresponding to wall shear stress values of 1, 3, 5, and 7 Pa. Cells were fixed using PBS containing 3% paraformaldehyde (PFA) for 10 min. Membranes were permeabilized with PBS containing 0.5% Triton X100 for 10 min. Then the system was rinsed with PBS. A first wash was with a solution of PBS containing 0.2% saponin and 2% BSA. A first antibody was used (human antipaxillin) for 30 min, followed by a second wash (same as before). The second antibody tetramethylrhodamine isothiocyanate (TRITC) was then used for 30 min under darkness conditions, followed by a third wash. The channel was then filled with a DAKO mounting medium. Microscopic observations were made using combined phase contrast and fluorescence, as shown in Fig. 6, where the first image is a phase-contrast image used for identification of cell contour thus providing the area and the location of the center of mass, whereas the second image shows the location of paxillin, which appears mainly at the cell edges through

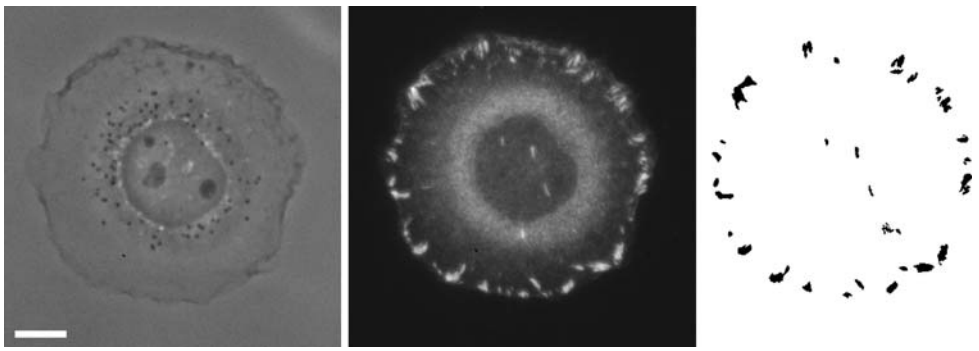

Fig. 6 Images of an adhering cell after application of successive stresses: phase contrast image, immunofluorescence image of the paxillin molecules, and corresponding focal adhesion zones obtained after image processing (maximum intensity levels only). The total number of adhesion zones is 31 and their average size is 2.5 μm^2, corresponding to a total adhesion area (sum) of 78 μm^2. The *white scale* bar represents 10 μm

several focal contacts. Fluorescence images were analyzed by using Image J software: brighter pixels were selected using a threshold method (Fig. 6). Finally, we used image processing to determine the number of adhesion zones (third image), their average area, and their total size. In the end the uncertainties on the focal adhesion areas were found to be around 10%.

Results

In order to understand how cells behave under flow conditions, we first need to have a reference, which is the spreading behavior with no applied flow. This will enable determination of relevant cell shapes and typical spreading times. Under static conditions, cells sediment, then they spread on the substrate (spreading does not occur at the same time for all cells). In most cases, spreading is fast and the maximum area is reached in less than 45 min as shown in Fig. 7a. After this spreading step, eventually followed by random migration on the substrate, some cells retract their protrusions (corresponding to the area decrease in Fig. 7a) to reach a round shape and divide into two daughter cells.

To take into account only viable cells, we decided to observe only daughter cells. Actually, a cell divides only when under good culture conditions, and cell division gives two healthy daughter cells. During the experiment under static conditions, 11 divisions were recorded, which means 22 daughter cells. For each division, the contour of the daughter cells was drawn and the cell areas were measured one hour after division. To decide which areas are to be selected, we determined the statistics of the population of daughter cells. The distribution of the areas of viable cells is shown in Fig. 8. Cell areas were in the range 800–1,600 μm^2. The mean area was 1,118 ± 248 μm^2. This is the range that we selected in our experiments.

T24 cells adherent at the bottom of microchannels were submitted to increasing shear flows. We observed a

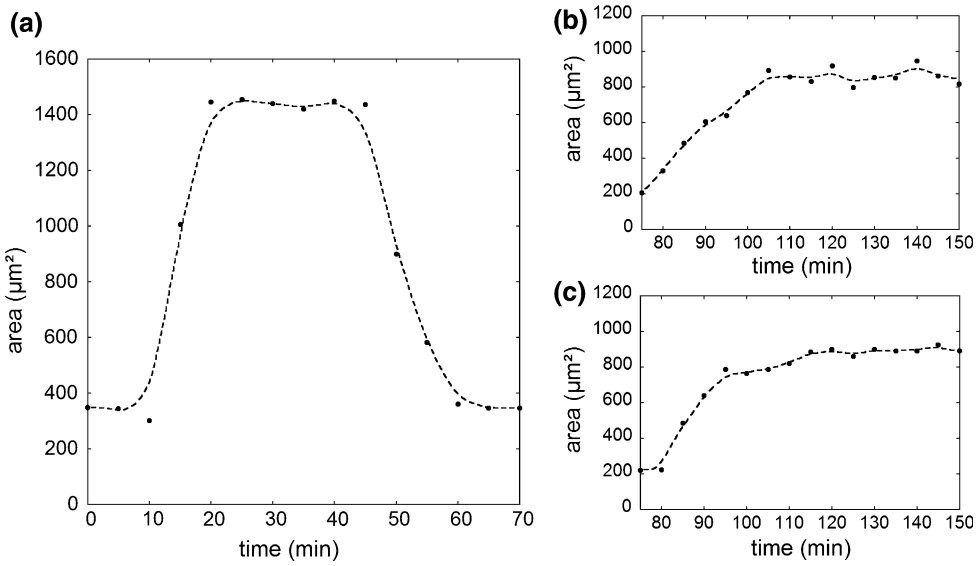

Fig. 7 T24 area under static conditions: **a** initial spreading is fast until reaching a plateau, then the area decreases just before cell division (time has been rescaled to $t = 0$ corresponding to the beginning of spreading). **b**, **c** Areas of the two daughter cells after the cell has divided. The *dashed lines* guide the eye

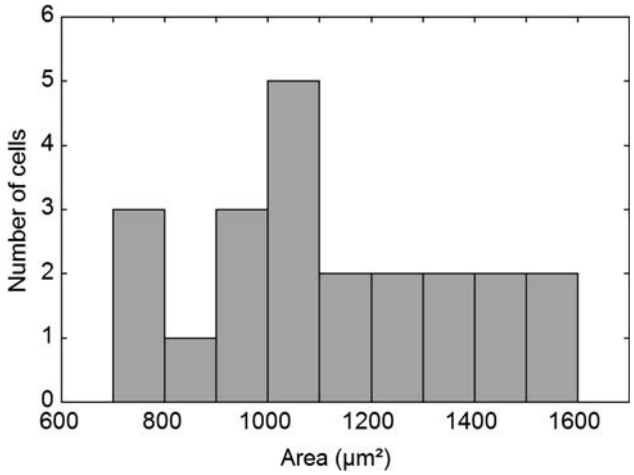

Fig. 8 Distribution of the areas of daughter cells under static conditions one hour after cell division

biphasic behaviour: cell area first increases at low WSS, then decreases for higher values of the WSS. Typical phase-contrast images are shown in Fig. 9. The cell first adheres and spreads along the channel wall as in Fig. 9a, b, while keeping a round shape with a prominent nucleus and a large lamellipodium around it. As the flow rate is increased (i.e. WSS increases), the cell area starts to decrease (Fig. 9c, d) until the cell eventually loses its adherence as shown in Fig. 9e just before detachment.

To analyze these data further, the time evolution of the area $A(t)$ of five cells is presented. Area versus time plots confirm that cell areas first increase at low WSS values (WSS values less than 3 Pa), as can be seen in Fig. 10, which illustrates the behavior of five cells under the same flow conditions. Let us try to compare this behavior with the static case. In the static experiments, cells are left to divide. Once they divide, they are round and spread rapidly for 15 mn (up to $A = 800$ μm^2 roughly as in Fig. 7b, c), then each daughter cell does not evolve in time very much (additional time of 50 mn). In the dynamic experiment, cells are first left to adhere for 15 mn; during this period they spread quite a bit (up to $A = 400-1{,}200$ μm^2). Then they are subjected to the increasing flow rates for 50 min. So the conditions are not exactly the same, but cells seem to spread more under flow conditions. Therefore, they increase their contact area by increasing their number of focal adhesion sites. This will be explained in what follows.

When the WSS is increased further, cell area increases slowly until the area reaches a maximum (as shown by the stars in Fig. 10). When the WSS increases further, the area decreases with time. The maximum area corresponds to a zero-slope for $\frac{dA}{dt}$, i.e. the transition between positive and negative values of the area rate of change $\frac{dA}{dt}$ (as shown for example in Fig. 11 where the slope is plotted against the applied WSS). From the polynomial fit and its derivative, we determine the slopes $\frac{dA}{dt}$. We assume a constant slope for each 5 min time interval during which a constant WSS is applied (0.1−29.6 Pa) as in the example shown in Fig. 11. The slope cuts the zero axis at a critical value of the WSS (WSS_c) corresponding to the maximum area (arrows in Fig. 11). Typical values of WSS_c are between 2 and 5 Pa, as shown in Fig. 12.

To investigate the effect of confinement, experiments were carried out (at least five cells) to measure mean ± SD of the WSS_c in channels with three different heights in the range 60−260 μm. Experimental data points in Fig. 12 represent average values of the WSS_c obtained in different microchannels whose heights were measured afterwards using SEM. Channel heights corresponding to one point were found to be slightly different, because of the UV exposure process used, but were within 5% maximum error. We found that WSS_c slowly increases when channel height increases as shown in Fig. 12. The three values that were chosen for the ratio R/h correspond to a narrow channel ($R/h \sim 0.2$), an intermediate one ($R/h \sim 0.1$), and a deep channel ($R/h \sim 0.06$), when using a cell height of approximately 15 μm. It is expected that a narrow channel will be more affected by the presence of the cell, acting as a blocking element, and that the velocity field will become 3D (Gaver and Kute 1988). This will affect the stresses exerted on the cell and, consequently, the resulting force

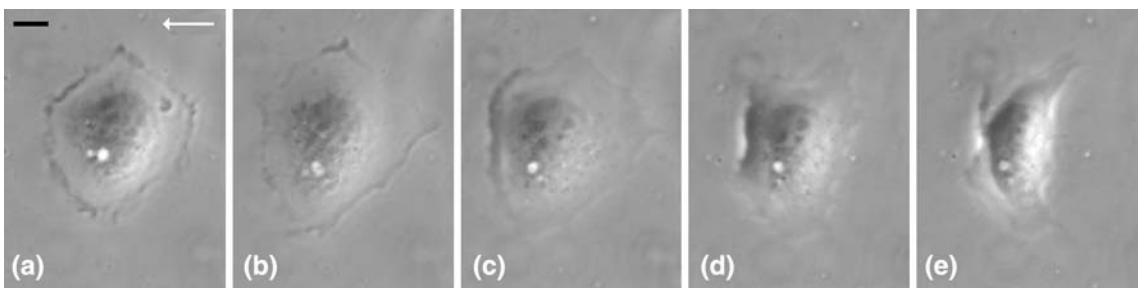

Fig. 9 Phase contrast images of a T24 cell adherent to the bottom of a microchannel ($w = 1$ mm, $h = 64$ μm) submitted to an increasing shear flow. The *white arrow* shows the flow direction. The *black scale* represents 10 μm. **a** WSS = 0.64 Pa, **b** WSS = 6.36 Pa, **c** WSS = 19.1 Pa, **d** WSS = 31.7 Pa, **e** WSS = 50.8 Pa

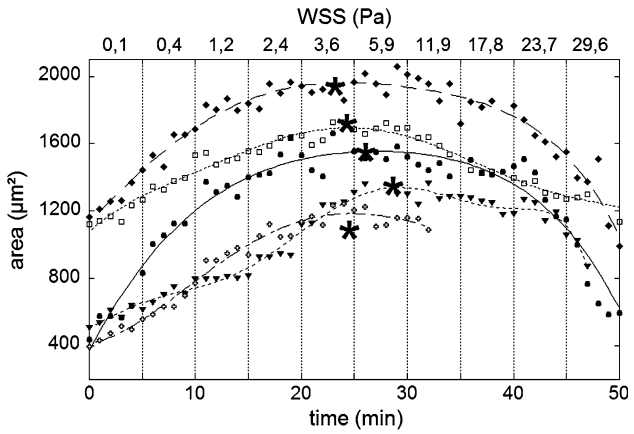

Fig. 10 Area evolution for five cells submitted to an increasing flow rate in a microchannel ($w = 1$ mm, $h = 61$ µm). Corresponding WSS are given on the top axis. *Symbols* represent experimental data (measured from phase-contrast images of the cells), which have been fitted by a standard polynomial fit (*lines*). For each fit, the *star* indicates the maximum area

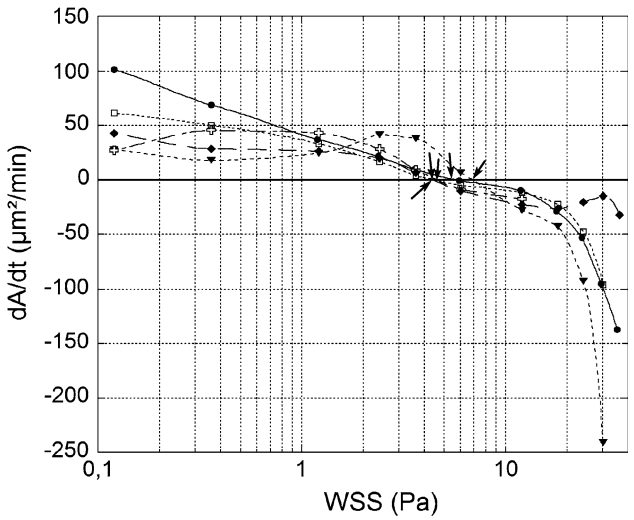

Fig. 11 Area change versus WSS for five cells submitted to an increasing flow rate in a microchannel ($w = 1$ mm, $h = 61$ µm). *Arrows* correspond to the location of the cell maximum

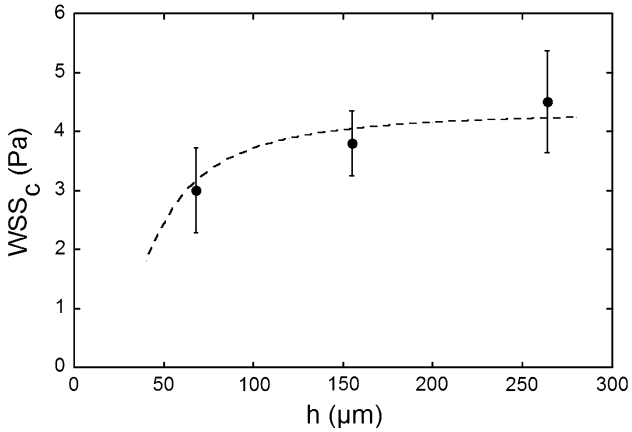

Fig. 12 WSS_c versus channel height h (at constant $w = 1$ mm). Data are the means of the WSS_c measured for all the cells tested in the experiments (10, 5, and 6 cells for the channels with average heights 68, 155, and 264 µm, respectively). The *dashed lines* are the fit of the results based on the model presented in the section "Modeling": Experimental values (*black dots*) are fitted with the hypothesis of equilibrium between adhesion and hydrodynamic forces: $F_{flow} = F_{ad_z}$. Results of the fit give: $Nf_{ad_z} = 12$ nN. *Error bars* are standard errors of the mean

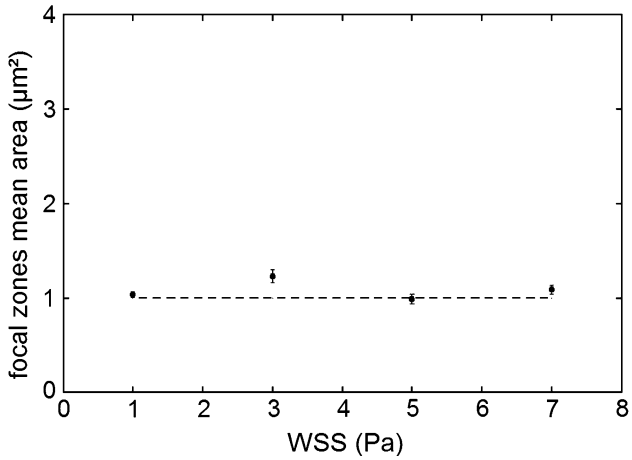

Fig. 13 Mean focal adhesions versus maximum shear stress experienced by cells adherent in microchannels ($w = 1$ mm, $h = 231$ µm). The flow rate, increased every 5 min, has generated an increasing wall shear stress: cells (35, 33, 24, and 31) were submitted to this increasing shear stress up to 1, 3, 5, and 7 Pa, respectively. The *dashed line* guides the eye. *Error bars* are standard errors of the mean

exerted by the flow field on the adherent cell. We note from Fig. 12 that for small heights h, the critical stress WSS_c for the onset of detachment becomes smaller, because of the above idea that a smaller stress is needed to generate a similar resultant force in a narrow channel. In the section "Modeling", we will use the model of Gaver and Kute (1988) to justify these data quantitatively.

In order to locate focal adhesions and study their evolution when fluid stress is increased, we carried out immunofluorescence experiments (see "Materials and methods") after fixing the T24-cells which have undergone different shear stresses. This enabled determination of the position and size of focal adhesion areas for cells fixed either after the first plateau at 1 Pa, or after the second plateau at 3 Pa, or the third at 5 Pa, or the last at 7 Pa. It appears clearly from these observations that focal adhesions are mostly located in the periphery of the cell, as shown in Fig. 6. The mean area of focal zones was nearly constant, around 1 µm^2, independent of the maximum shear stress the cell experienced (Fig. 13).

Our data in Fig. 14 show that the ratio of the area occupied by focal zones over the whole cell contact area is higher for cells sheared at 3 Pa. This wall shear stress value

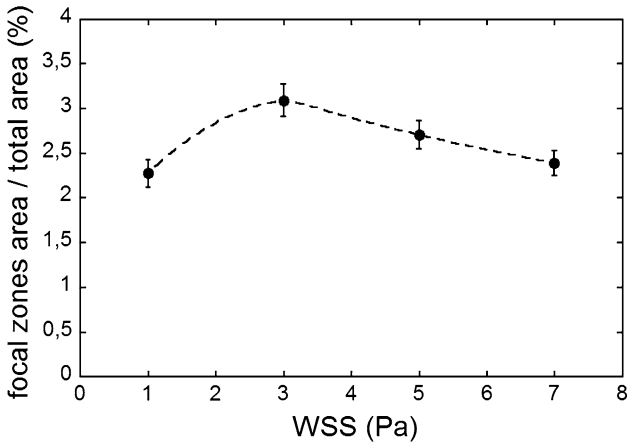

Fig. 14 Area fraction occupied by focal zones on adherent cells in microchannels ($w = 1$ mm, $h = 231$ μm) versus maximum shear stress experienced. The flow rate, increased every 5 min, has generated an increasing wall shear stress: 35, 33, 24, and 31 cells were submitted to shear stress up to 1, 3, 5, and 7 Pa, respectively. The *dashed line* guides the eye. *Error bars* are standard errors of the mean

is close to the critical wall shear stress obtained for cells in a channel of similar size (Fig. 12).

We then studied the spatial distribution of focal zones with respect to the direction of flow, that we chose to be the reference angle, as explained in Fig. 15.

Data treatment enabled determination of the total area corresponding to focal adhesions in each angular sector of 20°. Results have been plotted on the polar diagram in Fig. 16.

One can see the evolution and localization of the focal contacts around the cell, as the shear stress is increased:

- At low shear stress (1 Pa), focal zones represent between 2 and 3 μm^2 per angular sector of 20°, with no preferred direction.
- When the shear stress is increased further (up to 3 Pa), focal zones are located on the upstream side of the cell, which faces the flow, whereas at the back, their cumulative area decreases.
- Cells submitted to an increasing shear flow up to 5 Pa reinforce their focal adhesions on the lateral edges, where they reach nearly 5 μm^2.
- For the highest values of the shear stress (up to 7 Pa), focal adhesions are again located symmetrically with respect to the direction of flow, nonetheless their number decreases (about 2 μm^2 per angular sector of 20°).

Modeling

We need to correlate the WSS with the adhesion resistance, i.e. the forces generated by cells adhering to the wall to

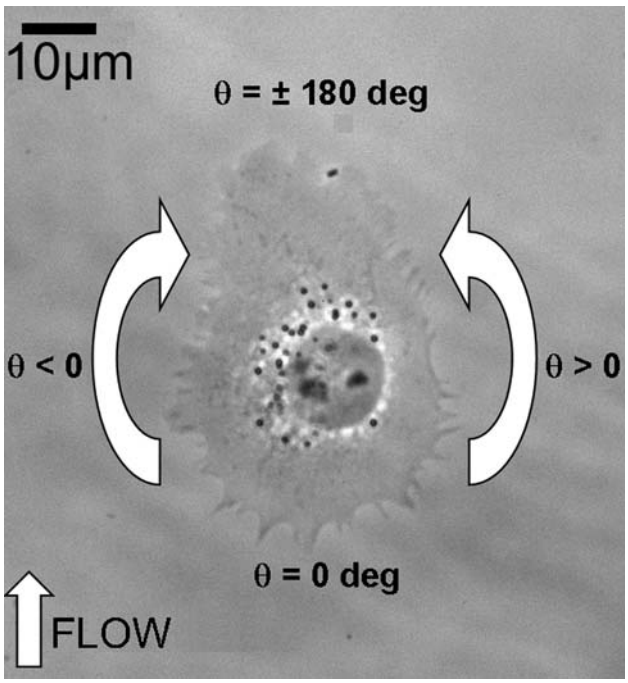

Fig. 15 Direction of flow and definition of the angle θ to locate the position of focal adhesion zones. $\theta = 0°$ corresponds to the point of the cell which faces the flow. θ takes values between 0 and $-180°$ on the *left part*, and 0 and 180° on the *right part*. Flow is from bottom to top, as indicated by the *arrow*

resist the flow. In confined geometries, the fluid is constrained by the channel walls, which leads to an increase in the flow resistance when an object partially blocks the channel (Fig. 2). Consequently, the full Navier–Stokes equations need to be solved for the components of the velocities, which now are in all three directions. This analysis was carried out in 2D (Gaver and Kute 1988) using the finite element method and lubrication theory predictions. The results obtained provide simple formulas for the force $\overrightarrow{F_{\text{flow}}}$ and torque $\overrightarrow{T_{\text{flow}}}$ applied to the cell, after integration of the full stress field over the cell boundary, considered as a semi-spherical bulge (radius R) attached to the bottom of a narrow channel (height h). The force and the torque values (around the axis going through the center of mass) induced by the flow have been generalized from 2D simulations to the 3D case (Gaver and Kute 1988). Explicit formulas for such force and torque are given by:

$$\overrightarrow{F_{\text{flow}}} = 24\eta\gamma^2 \frac{Q}{w} \frac{3.19 + 0.65\gamma + 4.34\gamma^2}{(1-\gamma^2)^{5/2}} \overrightarrow{e_z} \quad (5)$$

$$\overrightarrow{T_{\text{flow}}} = 12\pi\eta\gamma^2 \frac{RQ}{w} \frac{1.15 + 0.7\gamma}{(1-\gamma^2)^{5/2}} \overrightarrow{e_x} \quad (6)$$

where η is the fluid viscosity, R the cell radius, Q the flow rate, and $\gamma = \frac{R}{h}$ is the degree of confinement (h being the channel height). Several experimental situations have also shown that these formulas are quite accurate. The former

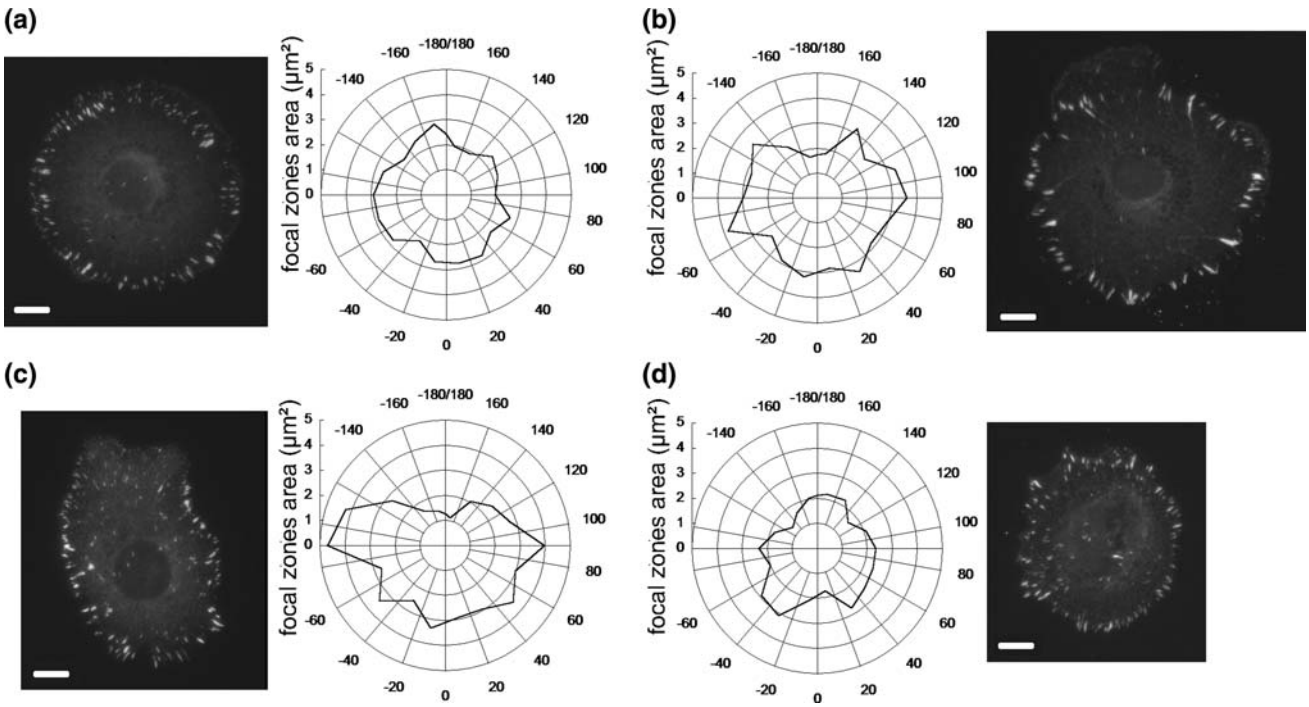

Fig. 16 Evolution of the mean angular localization of focal complexes for T24 adherent cells with increasing values of the wall shear stress: **a** 1 Pa, **b** 3 Pa, **c** 5 Pa, **d** 7 Pa. The cumulative area of the focal zones (averaged for 35, 33, 24, and 31 cells, respectively) is determined for each angular sector (20°). The orientation of the adhesion spots refers to the angle θ, whose origin corresponds to the cell locus facing the flow (Fig. 15). A typical fluorescent image (*scale bar* is 10 µm long) is shown as an example of the corresponding diagram

analysis (Gaver and Kute 1988) has been investigated further in recent years from a numerical point of view (Cao et al. 1998; Sugihara-Seki 2001; Wang and Dimitrakopoulos 2006), but not so much experimentally. It is important to realize that the "local shear stress" may take values much higher than the ones without the cell. In some cases like $R/h = 0.1$ for example (small obstruction), the shear stress at the top of the cell can be three times larger than the stress at the wall (Fig. 5 in Gaver and Kute 1988). This will have an effect on the total force $\overrightarrow{F_{\text{flow}}}$ which is already taken into account in Eq. 5, but this effect will not be as drastic as for the local stress.

Because the cell area decreases above a certain typical hydrodynamic force, we conclude that, above this typical value of the hydrodynamic stress, bonds are more likely to break than to form, leading to a decrease in total adhesive force. Thus there exists an equilibrium between the effect of hydrodynamic forces and adhesive forces, corresponding to the critical stress that was determined earlier. We will restrict our analysis to the influence of the force (and not the torque), as it seems that during the experiments, cells remain bound to the substrate and do not seem to be affected by lift effects, or at least not before the end when the ultimate detachment occurs. It is probably true that when the highest stresses (20−30 Pa) are involved, membrane "ruffling" and "peeling" of bonds may start, in

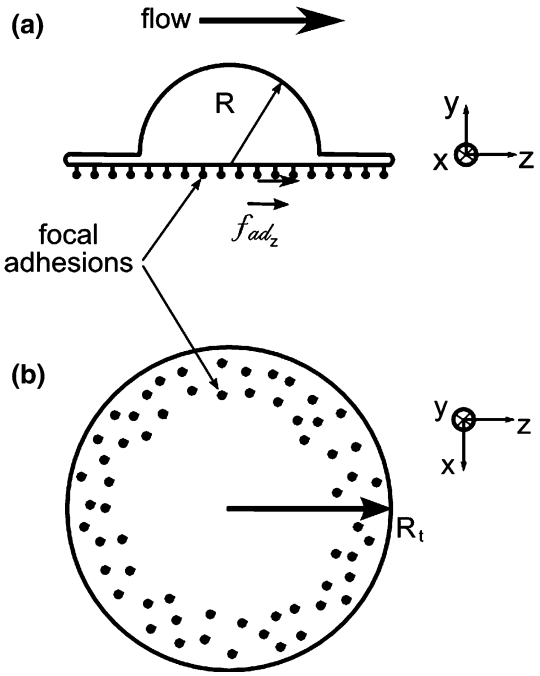

Fig. 17 Schematic views of a cell adhering to a flat surface submitted to a shear flow (flow is from left to right). **a** Side view: the cell is modeled as a half-sphere (radius R), with a circular lamellipodium (radius R_t). An adhesive force along z with magnitude F_{ad_z} is applied to each of the N focal adhesion sites. **b** Bottom view: *dots* represent focal adhesion sites, where the individual forces are exerted

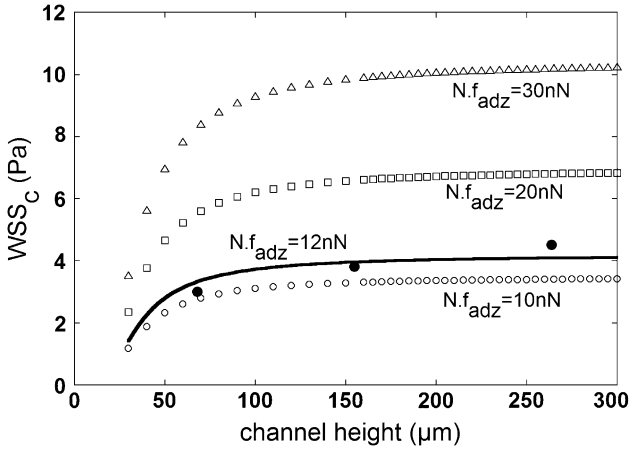

Fig. 18 WSS_c versus h calculated by use of Eq. 10 for different values of Nf_{ad_z} . $R = 15$ μm. Also shown are the data points and the best fit leading to $Nf_{ad_z} = 12$ nN

relation to the values of the torques. The hydrodynamic force is given in Eq. 5. The force due to the adhesive resistance of the cell that counterbalances the hydrodynamic force is now investigated. We consider a cell as a half-sphere of radius R, and assume a distribution of N adhesion sites on the whole cell–substrate contact area S, which is supposed to be circular (radius R_t). An estimate of R_t was obtained in the experiments $R_t \sim 26 \pm 2$ μm, as will be justified later. A force $\overrightarrow{f_{ad}}$ (which can be decomposed into a vertical component $f_{ad_y}\overrightarrow{e_y}$ and an horizontal component $f_{ad_z}\overrightarrow{e_z}$) is applied at each focal adhesion site (Fig. 17). The total adhesive force $\overrightarrow{f_{ad}}$ is the sum of the individual forces $\overrightarrow{f_{ad}}$: $\overrightarrow{F_{ad}} = \sum \overrightarrow{f_{ad}}$, and its components can be determined by summing the components of individual adhesive forces (Eq. 7):

$$\begin{cases} F_{ad_z} = \sum f_{ad_z} = Nf_{ad_z} \\ F_{ad_y} = \sum f_{ad_y} = Nf_{ad_y} \end{cases} \tag{7}$$

when in equilibrium, adhesion forces counterbalance hydrodynamic effects and the cell does not spread any longer but still holds on to the substrate, therefore the hydrodynamic force $\overrightarrow{F_{flow}}$, which is along the z axis ($\overrightarrow{F_{flow}} = F_{flow}\overrightarrow{e_z}$), is balanced by the horizontal component of the adhesion force F_{ad_z}:

$$F_{flow} = F_{ad_z} \tag{8}$$

Using the estimate of hydrodynamic force (Eq. 5) together with Eq. 8, the cell being represented by a semi-circular bulge of radius $R = 15$ μm, we then obtain, at equilibrium:

$$24\eta\left(\frac{R}{h}\right)^2\frac{Q}{w}\frac{3.19 + 0.65\frac{R}{h} + 4.34\left(\frac{R}{h}\right)^2}{\left(1-\left(\frac{R}{h}\right)^2\right)^{5/2}} = Nf_{ad_z} \tag{9}$$

where $WSS = 6\eta Q/wh^2$ appears and can be replaced by the shear stress at the wall (case without cell) from Eq. 4. The critical value of the WSS then becomes:

$$WSS_c = Nf_{ad_z}\frac{1}{4R^2}\frac{\left(1-\left(\frac{R}{h}\right)^2\right)^{5/2}}{3.19 + 0.65\frac{R}{h} + 4.34\left(\frac{R}{h}\right)^2} \tag{10}$$

The values of WSS_c versus h have been estimated for three values of the adhesion term $Nf_{ad_z} = 10$ nN, 20, and 30 nN using $R = 15$ μm. Results are shown in Fig. 18.

For small channels ($h < 100$ μm), the WSS increases rapidly with channel height h. The increase for higher channels is much slower and shows a plateau when h becomes large: $WSS_c = \frac{Nf_{ad_z}}{12.76R^2}$. This is in agreement with our experimental data: for the three channel sizes used in the experiments, WSS_c increases with h. Fitting of the experimental data with the results from the model (Eq. 10) has been carried out using Nf_{ad_z} as a variable (Fig. 18). Results give a good correlation (using $R = 15$ μm as an estimate of the cell height), corresponding to an approximate horizontal component of the adhesion force $F_{ad_z} = Nf_{ad_z} = 12$ nN.

Thus our modeling approach leads to the total adhesion force component in the plane corresponding to the cell–substrate contact $F_{ad_z} = 12$ nN. Although cell adhesion properties are cell and matrix-dependent (Young et al. 2007), estimates of the forces involved can be discussed. Different techniques have been elaborated to determine traction forces exerted by cells on a given substrate. For example, the displacement of fluorescent beads embedded in a soft polyacrylamide gel on to which cells adhere enables determination of the traction field, i.e. the local force per unit area (or per unit adhesion site) imposed by the cell. Maximum traction forces for T24 cells, HASM cells, and 3T3 fibroblasts spread on polyacrylamide gels (elasticity modulus in the range 1−10 kPa) have been found to be, respectively, 0.14 kPa (Ambrosi et al. 2009), 0.4 kPa (Butler et al. 2002), and 7 kPa (Dembo and Wang 1999). As it can be seen on fluorescence images (Paul et al. 2008; Bershadsky et al. 2003; Balaban et al. 2001), focal adhesion sizes are usually in the range (1−5 μm^2). These observations lead to traction forces between 0.05 and 10 nN per focal adhesion site. Note that in recent work (Das et al. 2008), measurements of traction forces ($\sim$0.25 kPa) were also made on L929 fibroblasts adhering in microchannels subjected to similar wall shear stresses in the range (1.5−4.7 Pa). Table 1 gives a summary of the different values available from this paper and the literature, usually stresses are available (i.e. binding force per unit area), therefore using the typical adhesion size of complexes from above one gets the binding force per focal adhesion (FA). Finally, the total binding force is obtained using an approximate number of 40 adhesion complexes (Paul et al. 2008).

Other studies using cells adhering to flexible micropillars give access to the same traction forces, correlated to focal adhesion sites located on the top of such micropillars.

Table 1 Available or estimated values of cell adhesion for different cell types using approximate focal adhesion (FA) sizes (1−5 μm^2)

	T24	T24	HSAM	3T3	L929
Ref.	This work	Ambrosi et al. (2009)	Butler et al. (2002)	Dembo and Wang (1999)	Das et al. (2008)
Gel elasticity	0.6 MPa	6.3 kPa	1.2 kPa	6.2 kPa	9.8 kPa
Total binding force	12 nN	5.5–28 nN	16-80 nN	280–1,400 nN	10–50 nN
Binding force per FA	0.27 nN	0.14–0.7 nN	0.4–2 nN	7–35 nN	0.25–1.25 nN
Stress	0.27 kPa	0.14 kPa	0.4 kPa	7 kPa	0.25 kPa

Fibroblasts and smooth muscle cells grown on such PDMS microposts develop cellular traction forces between 1 and 10 nN (Li et al. 2007; du Roure et al. 2005), whereas for individual epithelial cells migrating on micropillars (du Roure et al. 2005), maximal forces reached 3 nN. Although the present situation is not that of a migrating cell, it can be useful to compare the data given above to our case, because it is important to find out how much traction resistance a cell can exert on such a substrate. Based on the number of focal adhesions (40 on average) and their size (1 μm^2 as seen in Fig. 13), we can estimate the average force per focal site to be about 0.27 nN, or an equivalent stress of about 270 Pa at each focal adhesion site. If we now consider the analogy between the development of resistance stresses and the traction stresses developed during migration, it is probably true that the stresses obtained in the current study are typical ones at stable focal adhesions; they should be in the range of the maximum ones found during migration. Indeed, during migration, cells stop and rest, then they start pulling again and develop larger stresses from time to time (Ambrosi et al. 2009) after they have formed stable adhesions. The stresses found here are in the range of the maximum stresses found for migrating T24-cells (Ambrosi et al. 2009) on a 10 kPa substrate, where a maximum value of 200 Pa was found for the traction stress. In the present case, the PDMS Young's modulus used for the microchannel is roughly 0.6 MPa. Therefore, the microchannel results overestimate this value. Finally, let us note that the forces exerted by such cancer cells are rather small compared with those exerted by fibroblasts (Balaban et al. 2001). They compare better with values found for HASM cells (Butler et al. 2002).

Therefore our method of applying controlled shear forces using a flow field combined with fluorescent microscopy is quite powerful. It can lead to determination of traction resistance exerted by the cell through its focal contacts.

Conclusions

A microfluidics experiment has been carried out to detach cancer cells adhering to the bottom of a micro-fabricated channel. Analysis of cell morphology clearly revealed resistance of the cell to increasing flow, until a critical stress was reached. This critical stress is a function of the product of the number of adhesion sites, their strength, and the confinement ratio. When confinement increases, the critical shear stress decreases, whereas it reaches a constant limit for high channels. This rather simple experiment was combined with fluorescence assays to enable determination of the forces developed at each focal adhesion site. Although this analysis contains estimates, it can predict adhesion rather well compared with previous studies related to traction forces exerted by adhering/migrating cells. It also confirms a previous result showing that such cancer cells exert small forces, therefore they may move faster. Further fluorescence studies are now needed to correlate more precisely the temporal and spatial distribution of adhesion sites (size, number) as a function of the applied shear stress.

Acknowledgments The authors thank the European Commission Marie Curie Research Training Network MRTN-CT-2004-503661 "Modeling, mathematical methods and computer simulation of tumor growth and therapy" for its support. Image acquisition was performed using the microscopy facility at the "Institut Albert Bonniot". This equipment was partly funded by "Association pour la Recherche sur le Cancer" (Villejuif, France) and the "Nanobio program". We are also thankful to V. M. Laurent for helpful discussions and reading of the manuscript.

References

Ambrosi D, Duperray A, Peschetola V, Verdier C (2009) Traction patterns of tumor cells. J Math Biol 58:163–181

Balaban NQ, Schwarz US, Riveline D, Goichberg P, Tzur G, Sabanay I, Mahalu D, Safran S, Bershadsky A, Addadi L, Geiger B (2001) Force and focal adhesion assembly: a close relationship studied using elastic micro-patterned substrates. Nat Cell Biol 3:466–472

Bershadsky AD, Balaban NQ, Geiger B (2003) Adhesion-dependent cell mechanosensitivity. Annu Rev Cell Dev Biol 19:677–695

Bohnet S, Ananthakrishnan R, Mogilner A, Meister JJ, Verkhovsky AB (2006) Weak force stalls protrusion at the leading edge of the lamellipodium. Biophys J 90:1810–1820

Butler JP, Tollic-Norrelykke IM, Fabry B, Fredberg J (2002) Traction fields, moments, and strain energy that cells exert on their surroundings. Am J Physiol 282:C595–C1605

Cao J, Donell B, Deaver DR, Lawrence MB, Dong C (1998) In vitro side-view imaging technique and analysis of human T-leukemic

cell adhesion to ICAM-1 in shear flow. Microvasc Res 55:124–137
Chachisvilis M, Zhang YL, Frangos JA (2006) G-protein coupled receptors sense fluid shear stress in endothelial cells. Proc Natl Acad Sci USA 103:15463–15468
Chaw KC, Manimaran M, Tay EH, Swaminathan S (2007) Multi-step microfluidic device for studying cancer metastasis. Lab Chip 7:1047–1047
Chen CS (2008) Mechanotransduction—a field pulling together. J Cell Sci 121:3285–3292
Chotard-Ghodsnia R, Drochon A, Faucheux N, Nagel MD, Grebe R (2002) Effect of shear stress and of transmural pressure on cAMP-dependent responses of cells adhering to a biomaterial. Eur Phys J AP 17:155–162
Chotard-Ghodsnia R, Haddad O, Leyrat A, Drochon A, Verdier C, Duperray A (2007) Morphological analysis of tumor cell/endothelial cell interactions under shear flow. J Biomech 40:335–344
Coughlin MF, Schmid-Schönbein GW (2004) Pseudopod projection and cell spreading of passive leukocytes in response to fluid shear stress. Biophys J 87:2035–2042
Dalous J, Burghardt E, Müller-Taubenberger A, Bruckert F, Gerisch G, Bretschneider T (2008) Reversal of cell polarity and actin–myosin cytoskeleton reorganization under mechanical and chemical stimulation. Biophys J 94:1063–1074
Das T, Maiti TK, Chakraborty (2008) Traction force microscopy on-chip: shear deformation of fibroblast cells. Lab Chip 8:1308-1318
De R, Zemel A, Safran SA (2007) Dynamics of cell orientation. Nat Phys 3:655–659
Decave E, Garrivier D, Bréchet Y, Fourcade B, Brückert F (2002) Shear flow-induced detachment kinetics of dictyostellium discoideum cells from solid substrate. Biophys J 82:2383–2395
Dembo M, Wang YL (1999) Stresses at the cell-to-substrate interface during locomotion of fibroblasts. Biophys J 76:2307–2316
Discher DE, Janmey P, Wang Y (2005) Tissue cells feel and respond to the stiffness of their substrate. Science 310:1139–1143
Duffy DC, Cooper McDonald J, Schueller OJA, Whitesides GM (1988) Rapid prototyping of microfluidic systems in poly(dimethylsiloxane). Anal Chem 70:4974–4984
du Roure O, Saez A, Buguin A, Austin RH, Chavrier P, Silberzan P, Ladoux B (2005) Force mapping in epithelial cell migration. Proc Natl Acad Sci USA 102:2390–2395
Gaver DP, Kute SM (1988) A theoretical model study of the influence of fluid stresses on a cell adhering to a microchannel wall. Biophys J 75:721–733
Gutierrez E, Groisman A (2007) Quantitative measurements of the strength of adhesion of human neutrophils to a substratum in a microfluidic device. Anal Chem 79:2249–2258
Hammer DA, Lauffenburger DA (1987) A dynamical model for receptor-mediated cell adhesion to surfaces. Biophys J 52:475–487
Ingber DE (2003) Mechanobiology and diseases of mechanotransduction. Ann Med 35:564–577
Irima D, Charras G, Agrawal N, Mitchison T, Toner M (2007) Polar stimulation and constrained cell migration in microfluidic channels. Lab Chip 7:1783–1790
Jin Q, Verdier C, Singh P, Aubry N, Chotard-Ghodsnia R, Duperray A (2007) Migration and deformation of leukocytes in pressure driven flows. Mech Res Commun 34:411–422
Kwon KW, Choi SS, Lee SH, Kim B, Lee SN, Park MC, Kim P, Hwang SY, Suh KY (2007) Label-free, microfluidic separation and enrichment of human breast cancer cells by adhesion difference. Lab Chip 7:1461–1468
Lawrence MB, Springer TA (1991) Leukocytes roll on a selectin at physiological flow rates: distinction from and prerequisite for adhesion through integrins. Cell 65:859–873
Li B, Xie L, Starr ZC, Yang Z, Lin JL, Wang JHC (2007) Development of micropost force sensor array with culture experiments for determination of cell traction forces. Cell Motil Cytoskelet 22:509–518
Lo CM, Wang HB, Dembo M, Wang YL (2000) Cell movement is guided by the rigidity of the substrate. Biophys J 79:144–152
Lu H, Koo LY, Wang WM, Lauffenburger DA, Griffith LG, Jensen KF (2004) Microfluidic shear device for quantitative analysis of cell adhesion. Anal Chem 76:5257–5264
Moazzam F, DeLano FA, Zweifach B, Schmid-Schönbein GW (1997) The leukocyte response to fluid stress. Proc Natl Acad Sci USA 94:5338–5343
Orr AW, Helmke BP, Blackman BR, Schwartz MA (2006) Mechanisms of mechanotransduction. Dev Cell 10:11–20
Paul R, Heil P, Spatz JP, Schwartz US (2008) Propagation of mechanical stress through the actin cytoskeleton toward focal adhesions: model and experiment. Biophys J 94:1470–1482
Pierres A, Benoliel AM, Bongrand P (1995) Measuring the lifetime of bonds made between surface-linked molecules. J Biol Chem 270:26586–26592
Pozrikidis C (1997) Shear flow over a protuberance on a plane wall. J Eng Math 31:29–42
Reinhart-King CA, Dembo M, Hammer DH (2005) The dynamics and mechanics of endothelial cell spreading. Biophys J 89:676–689
Riveline D, Zamir E, Balaban NQ, Schwarz US, Ishizaki T, Narumiya S, Kam Z, Geiger B, Bershadsky AD (2001) Focal contacts as mechanosensors: externally applied local mechanical force induces growth of focal contacts by an mDia1-dependent and ROCK-independent mechanism. J Cell Biol 153:1175-1186
Saadi W, Wang SJ, Lin F, Jeon NL (2006) A parallel-gradient microfluidic chamber for quantitative analysis of breast cancer cell chemotaxis. Biomed Microdev 8:109–118
Schwartz MA, DeSimone DW (2008) Cell adhesion receptors in mechanotransduction. Curr Opin Cell Biol 20:551–556
Sugihara-Seki M (2001) Flow around cells adhered to a microvessel wall. II: comparison to flow around adherent cells in channel flow. Biorheology 38:3–13
Théry M, Racine V, Piel M, Pépin A, Dimitrov A, Chen Y, Sibarita J, Bornens M (2006) Anisotropy of cell adhesive microenvironment governs cell internal organization and orientation of polarity. Proc Natl Acad Sci USA 103:19771-19776
Thoumine O, Ziegler T, Girard PR, Nerem RM (1995) Elongation of confluent endothelial cells in culture: the importance of fields of force in the associated alterations of their cytoskeletal structure. Exp Cell Research 219:427–441
Verdier C (2003) Review. Rheological properties of living materials: From cells to tissues. J Theor Med 5:67–91
Verdier C, Couzon C, Duperray A, Singh P (2009) Modeling cell interactions under flow. J Math Biol 58:235–259
Wang Y, Dimitrakopoulos P (2006) Nature of the hemodynamic forces exerted on vascular endothelial cells or leukocytes adhering to the surface of blood vessels. Phys Fluids 18:087107
Wankhede SP, Du Z, Berg JM, Vaughn MW, Dallas T, Cheng KH, Gollahon L (2006) Cell detachment model for an antibody-based microfluidic cancer screening system. Biotechnol Prog 22:1426–1433
White FM (2003) Fluid mechanics. McGraw–Hill, New York
Young EWK, Wheeler AR, Simmons CA (2007) Matrix-dependant adhesion of vascular endothelial cells in microfluidic channels. Lab Chip 7:1759–1766